NATIONAL AERONAUTICS AND SPACE ADMINISTRATION

Technical Memorandum 33-557

Part I

Junction Characteristics of Silicon Solar Cells

Nonilluminated Case

Richard J. Stirn

JET PROPULSION LABORATORY
CALIFORNIA INSTITUTE OF TECHNOLOGY
PASADENA, CALIFORNIA

August 15, 1972

NATIONAL AERONAUTICS AND SPACE ADMINISTRATION

Technical Memorandum 33-557

Part I

Junction Characteristics of Silicon Solar Cells

Nonilluminated Case

Richard J. Stirn

JET PROPULSION LABORATORY
CALIFORNIA INSTITUTE OF TECHNOLOGY
PASADENA, CALIFORNIA

August 15, 1972

Prepared Under Contract No. NAS 7-100
National Aeronautics and Space Administration

PREFACE

The work described in this report was performed by the Guidance and Control Division of the Jet Propulsion Laboratory.

ACKNOWLEDGMENTS

The author should like to thank W. Hermann and N. Massie for preparing the samples and obtaining some of the data, and J. Devaney for the scanning electron microscope pictures. He also should like to thank P. Iles of Centralab and E. Ralph of Heliotek for supplying the solar cells.

CONTENTS

TABLES

FIGURES

ABSTRACT

Precise values of the reverse saturation currents in 2- and 10-Ω-cm silicon solar cells and magnitudes of the diffusion and recombination components have been obtained. The recombination current as well as leakage current due to shunting are shown to be nonuniform across the cell. The diffusion lengths calculated from the diffusion current components agree well with diffusion lengths measured independently in similar material. Models are given demonstrating the effect of recombination and shunting currents on the dark current-voltage characteristics of solar cells.

I. INTRODUCTION

Over the years the silicon solar cell has evolved into a highly reliable device with characteristics that, for the most part, are well understood and generally predictable over the range of space environments between Mars and Venus. However, even with these relatively restricted environments, there is a large discrepancy (about a factor of two) between the ideal conversion efficiency predicted by semiempirical derivations and the efficiencies actually achieved by the finished devices. In addition, missions using solar cells in regions beyond the orbit of Mars, such as solar electric propulsion missions to individual asteroids or comets and possibly missions to Jupiter and its satellites, will require cell operation at much lower temperatures and light intensities than normally encountered.

For obtaining maximum conversion efficiency in solar cells, the electrical performance of the p/n junction is second in importance only to high minority carrier lifetimes. With the decreasing light intensities and temperatures found in the missions mentioned above, this secondary importance becomes much more important. As will be discussed in more detail in a future report, (JPL Technical Memorandum 33-557, Part II: Illuminated Case), the magnitude of the junction current at a given voltage when the junction is forward biased, as it is in the photovoltaic mode, is important in determining the cell efficiency. Excessive current degrades the power output by reducing the cell curve factor and the voltage output. The lower the solar intensity incident upon the cell, the larger the relative amount of degradation.

Previously reported measurements have given widely varying and erroneous values of the junction current parameters due to series resistance effects, to the presence of localized current-shunting paths, and, as shall be shown, to the presence of two parallel conduction processes. The latter effect was recognized by Wolf and Rauschenback (Ref. 1) nearly ten years ago for p on n solar cells and was described as a double exponential current-voltage (I-V) characteristic.

This report (Part I) presents precise values of the junction current parameters for both 2- and 10-Ω-cm n on p cells obtained by measuring the dark forward I - V curves over a wide range of temperatures (393 to 145 K), eliminating the shunt resistance problem by etching the solar cell to form an array of small area mesas. Use of the small areas also lowers the series resistance considerably by essentially eliminating the sheet resistance in the diffused (<0.5 μm) top layer of the solar cell. This allowed measuring more than ten times the usual amount of current density with a negligible amount of voltage drop across the series resistance. Models are given demonstrating the relative influence of both shunting effects and the magnitude of the second current conduction process (due to recombination in the space-charge region) on the total forward I - V characteristics. Also discussed are possible causes for the ubiquitous shunting paths and some preliminary results of a scanning electron microscope investigation of them.

A second report (Part II) will relate the findings of Part I to the photovoltaic mode of operation and show how the various mechanisms of conduction affect the solar cell power output and efficiency at different light intensities and temperatures.

II. THEORY

Under illumination, a photovoltaic device provides a current by the generation of electron-hole pairs — nearly one pair for each photon absorbed, having an energy greater than the energy of the band gap.

The output current consists of those minority carriers ultimately collected by a suitable energy barrier before being lost through recombination. The barrier can be either a p/n junction or a Schottky barrier, i.e., a metal film-semiconductor device. In either case, the device can be represented as a diode in parallel with a current generator, as shown in Fig. 1. A shunting current

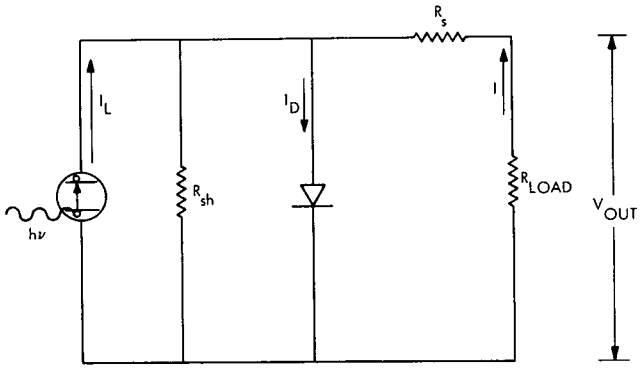

Fig. 1. Equivalent circuit for a solar cell

seems to exist in all solar cells to some degree, and can be represented as an ohmic resistor R_{sh} in parallel with the diode. The output current through the load resistance I is then simply

$$I = I_D - I_L \tag{1}$$

where I_L is the light generated current furnished by the collected minority carriers, and I_D is the diode current that flows in the opposite direction to I_L because of the forward potential developed across the cell. It is this diode current for p/n junction solar cells that is the subject of this report.

A. Diffusion Model

Most monographs on solar cells treat the diode current as expressed by the simple Shockley diffusion current relation (Refs. 2 and 3)

$$I_D = I_{01}\left[\exp\left(qV_D/A_1kT\right) - 1\right] \tag{2a}$$

where

$$I_{01} = \frac{qD_P}{L_P}\frac{n_i^2}{N_D} + \frac{qD_n}{L_n}\frac{n_i^2}{N_A} \tag{2b}$$

is referred to as the reverse saturation current.[1] In these expressions, q is the charge of the electron; k is the Boltzmann constant; T is the absolute temperature; A_1 is an empirical factor to be discussed below; D and L are the diffusion constant and diffusion length, respectively, with the subscripts n and p referring to the n-doped and p-doped sides of the junction, respectively; N_D and N_A are the donor and acceptor concentrations that are assumed fully ionized, and n_i is the intrinsic carrier concentration

$$n_i = \sqrt{N_c N_v}\exp\left(-E_g/2kT\right) \tag{3}$$

In Eq. (3), N_C and N_V are the density-of-states in the conduction and valence bands, respectively, and E_g is the energy of the band gap. For silicon, the intrinsic carrier concentration can be written as

$$n_i = 2.4 \times 10^{19}\left(\frac{T}{300K}\right)^{3/2}\exp\left(-\frac{0.56}{kT}\right)\ \text{cm}^{-3}$$

The ratio $n_i^2/N_{D,A}$ in Eq. (26) is the number of minority carriers in the n and p regions, respectively, due to thermal excitation, not light excitation. The diffusion process in silicon solar cells is such that an abrupt junction with a highly doped n-type region is formed on a lightly doped p-type base. Thus the first term in Eq. (2b) can be neglected because of the small number of minority holes in the diffused region (high N_D). Since the diffusion length L_n is equal to $\sqrt{D_n \tau_n}$, where τ_n is the minority carrier (electron) lifetime,

$$I_{01} \simeq q\sqrt{\frac{D_n}{\tau_n}}\frac{n_i^2}{N_A} \tag{2c}$$

for n on p solar cells. Since the temperature dependence of the quantities in Eq. (2c) is negligible compared to the exponential term in n_i, the temperature dependence of the reverse saturation current due to diffusion I_{01} should be exponential with the band gap energy.

The voltage across the diode V_D in Eq. (2) is related to the external voltage V by

$$V_D = V \pm IR_s \tag{4}$$

where R_s is the series resistance of the device. In the photovoltaic mode, the external voltage is smaller than the voltage across the junction V_D (+ sign), while in the dark with applied forward voltage, the voltage V_D is less than the applied voltage V by the amount of the drop across R_s (- sign).

The use of the diffusion current [Eqs. (2)] with Eq. (1) allowed other expressions to be derived rather simply, such as expressions (Refs. 4, 5) for the voltage at maximum power point, output power, efficiency, and open-circuit voltage — the latter, for instance, given by

$$V_{oc} = \frac{A_1kT}{q}\ln\left(I_L/I_{01} + 1\right) \tag{5}$$

However, it has long been recognized that the measured values of the reverse saturation current are far larger than those predicted by

[1] All references to currents in this report are actually current densities.

Eq. (2b) and also that an empirical factor called the "A-factor" is needed in the denominator of the exponential in Eq. (2a). The values of this "A-factor" that have been reported for solar cells vary between 1.0+ to 4 or 5, whereas the theoretical value of A_1 in the Shockley diffusion theory is 1.0.

B. Recombination Model

For some time, it has been recognized that a second component to the diode current can exist — current due to generation and recombination of carriers via centers within the band gap in the space-charge region of a p/n junction. With the simplifying assumption of single-level uniformly-distributed centers at the center of the band gap, the I - V relationship can be written as (Refs. 6, 2, 3)

$$I_D = I_{02}\left[\exp\left(\frac{qV_D}{A_2kT}\right) - 1\right] \qquad (6)$$

where the maximum theoretical value of A_2 is 2.0. The reverse saturation current for this idealized case is given by

$$I_{02} = \frac{qWn_i}{2\tau_0} \qquad (7)$$

where W is the width of the space-charge region as determined by capacitance measurements, and $\tau_0 \equiv \tau_n = \tau_p$. The effective minority lifetime τ_0 is related to the density of recombination centers N_t and to the center's capture cross section σ by

$$1/\tau_0 = \sigma v_{th} N_t$$

where v_{th} is the thermal velocity of the semiconductor. The temperature dependence of n_i is dominated by the exponential [Eq. (3)], and since I_{02} is linearly dependent on n_i, the temperature dependence of the reverse saturation current due to recombination (I_{02}) should be exponential with one-half of the band gap energy.

The factor A_2 in Eq. (6) can be less than 2.0 if the assumption that the recombination centers are exactly at the middle of the band gap is lifted. The expression for I_{02} given by Eq. (7) should be multiplied by a complicated factor involving the depth of the center (Ref. 6). When the center is energetically away from the middle of the band gap, we may have $1 < A_2 < 2$ depending on the forward applied bias. This more complicated situation will not be pursued at this time.

Many reported values of the empirical A-factor in silicon solar cells have been greater than two. One mechanism has been proposed that allows for $2 < A < 4$ (Ref. 7), that of carrier recombination in a surface channel in amounts larger than the bulk recombination. However, it will be shown in this report that the cause of the high values of A measured in earlier studies was probably due to the presence of ohmic shunting currents that are unavoidably present in the large-area shallow junctions used in solar cells.

C. Combined Model

Since the experiments discussed below demonstrate the existence of both diffusion and space-charge recombination current in silicon solar cells, the proper diode characteristic equation is

$$I_D = I_{01}\left[\exp\left(\frac{qV_D}{A_1kT}\right) - 1\right] + I_{02}\left[\exp\left(\frac{qV_D}{A_2kT}\right) - 1\right] + V_D/R_{sh} \qquad (8)$$

where R_{sh} is the shunt resistance shown in Fig. 1, and I_{01}, I_{02}, and V_D are given by Eqs. (2b), (7), and (4), respectively. Therefore, both components are separately stated rather than the simpler expression [Eq. (2a)] used with an average A-factor reflecting the relative contributions of each current component.

To better understand the effect of the three current components in Eq. (8) on the dark forward bias ($V > 0$) of a solar cell, Eq. (8) was graphed for various combinations of I_{01}, I_{02}, and R_{sh}. Similar modeling for the illuminated solar cell using Eq. (1) in addition to Eq. (8) will be presented in a following report (Part II). Figure 2 shows the effect at room temperature of varying amounts of recombination current without the presence of current shunting, while Figs. 3 and 4 show the effect of shunting for relatively low (10^{-8} A/cm^2) and relatively high (10^{-6} A/cm^2) recombination current density, respectively.

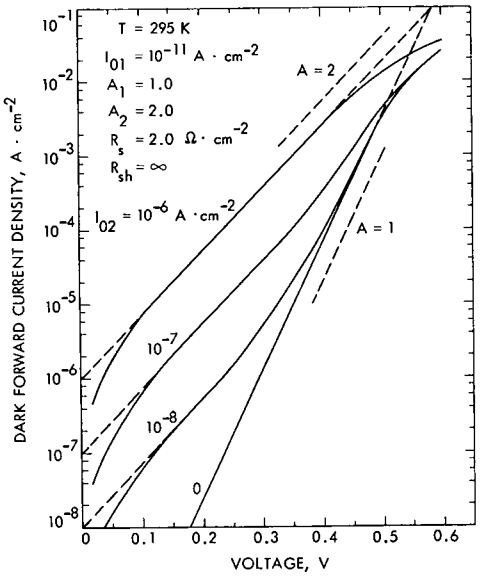

Fig. 2. Ideal dark forward current-voltage characteristic at room temperature showing effect of recombination current

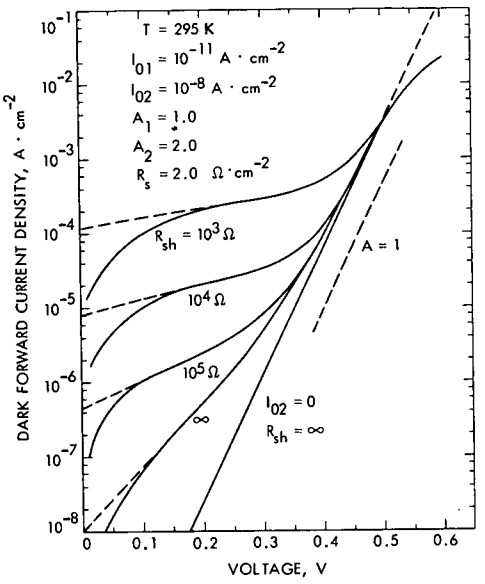

Fig. 3. Ideal dark forward current-voltage characteristic at room temperature showing effect of shunting with $I_{02} = 10^{-8}$ A · cm^{-2}

Figures 2-4 were drawn for the diffusion current expected in 10-Ω-cm silicon ($I_{01} = 10^{-11}$ A · cm^{-2}). The value of R_s is typical for present day solar cells. From these figures we see that shunting has little effect when the recombination current is relatively important, such as was probably the case with solar cells made in the 1950's and early 1960's, and as should also be the case for solar cells that have been damaged by particle irradiation. The presence of the recombination current affects the I - V characteristic over the entire voltage range -- not just the low voltage region. This is particularly so the lower the temperature, as shown in Fig. 5. The latter figure also shows that shunting is relatively much more important at lower temperatures. This occurs because the shunting current is essentially temperature independent while I_{01} and I_{02} fall off exponentially with temperature. Since I_{01} falls off more rapidly (n_i^2 as compared to $I_{02} \propto n_i$), the relative effect of the recombination current is much more pronounced at lower temperatures even at higher voltages. Similarly, at a fixed temperature, the wider the band gap of the semiconductor, the smaller the role of diffusion current.

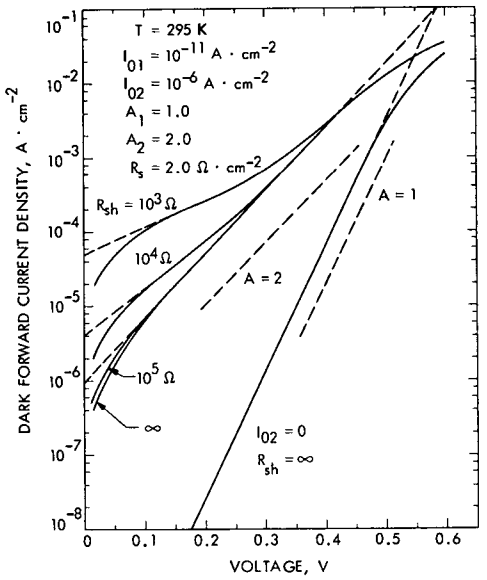

Fig. 4. Ideal dark forward current-voltage characteristic at room temperature showing effect of shunting with $I_{02} = 10^{-6}$ A · cm^{-2}

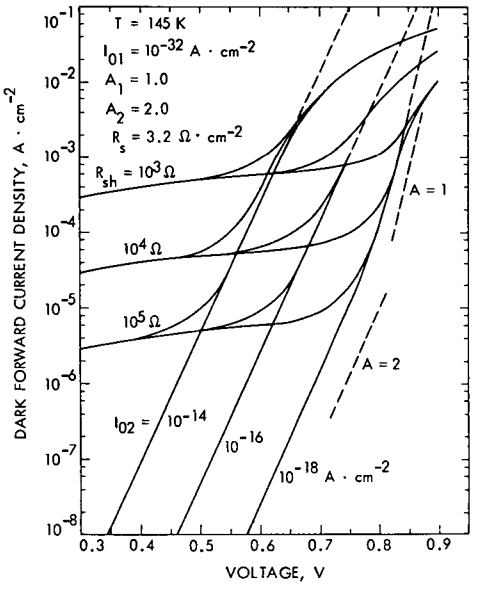

Fig. 5. Ideal dark forward current-voltage characteristic at 145 K showing effect of recombination current and shunting

III. EXPERIMENTAL TECHNIQUES

The silicon solar cells used in this study of the dark I - V characteristics were 2- and 10-Ω-cm n on p cells supplied by Centralab Semiconductor Division of Globe Union, Inc., and by Heliotek Division of Textron, Inc. The cells, except for some specially prepared ones discussed below, were typical cells obtained from the production line except that no anti-reflection coatings were applied. Besides I - V and capacitance measurements on the entire area (2 × 2 cm), similar measurements were performed on small diameter (~1 mm) mesas that were formed by etching several microns of silicon from the diffused surface with 1:10 HF/HCl acids. Only under wax dots placed over grid lines were areas of the p/n junction left remaining (Fig. 6) – the remaining grid line serving as a convenient contact.

The below room-temperature measurements were performed at 145, 192, 232, and 273 K by using various Freon baths in a vacuum dewar, and above room-temperature measurements were performed at 335 and 393 K using an electrical heater. In both cases, the sample was in a vacuum while contacted to a metal finger held at the desired temperature. The range of temperatures selected covers the range experienced by solar panels heated by solar energy between the orbits of Jupiter and Venus. Cells that showed Schottky barrier effects at the back contact were not used in this study.

Although the technique of measuring the I - V characteristics is straightforward, extreme care was required with mesas to avoid leakage currents, ground loops, and the effects of voltmeter current flow because of the low currents utilized (down to 10^{-9} A). These effects are negligible with the full cell area because shunting usually keeps the current level two to three orders of magnitude higher. The use of batteries for applied voltages and battery-operated meters greatly aided in solving the grounding problems. Voltages were measured with a digital Fluke multimeter, Model 8120A, and currents with a Keithley electrometer, either Model 610B or 600B, measuring five points per decade of current. The data were least squares fitted to a two-exponential model as given by Eq. (8) without the shunt term.[2] With a curve fitting technique, the values of A_1, A_2, I_{01}, I_{02}, and R_s as well as the last four quantities with a fixed value of one for A_1 were determined. This technique is being modified to give also a fit to the two-exponential curve with shunting. Capacitance measurements were performed with a Boonton Bridge, Mode 74C-58 (100 kHz). Background doping in the base region was determined by the voltage dependence of the capacitance and the widths of the space-charge regions were obtained from the zero bias values of the capacitance (Refs. 2, 3).

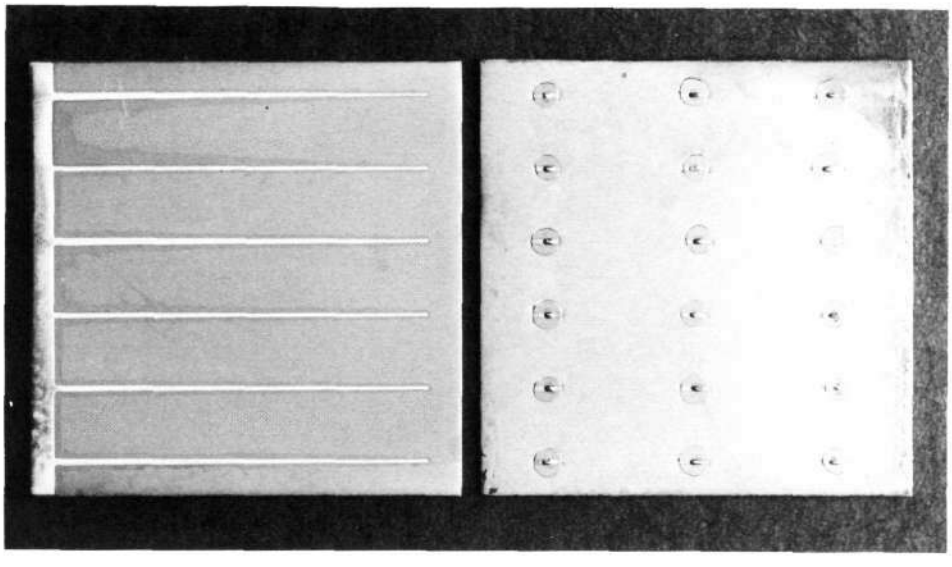

Fig. 6. Photograph of a standard solar cell and of a cell etched into small-area mesas

[2] Computer program kindly supplied by M. Wolf.

IV. EXPERIMENTAL RESULTS

A. Current-Voltage Characteristics

When one examines typical solar cell dark forward current-voltage characteristics such as those given in Figs. 7a and 7b for 2- and 10-Ω-cm cells, respectively, the most striking feature is the variability of the curve shapes in the low to middle voltage range. The variability of up to two decades of current for a fixed voltage between 0.1 to 0.3 V is due to different amounts of shunt resistance and recombination current in the junction region that are impossible to separate. The models presented in Section II showed how each mechanism can affect the entire characteristic and how difficult it can be to separate the two mechanisms depending on the relative amount of either one.

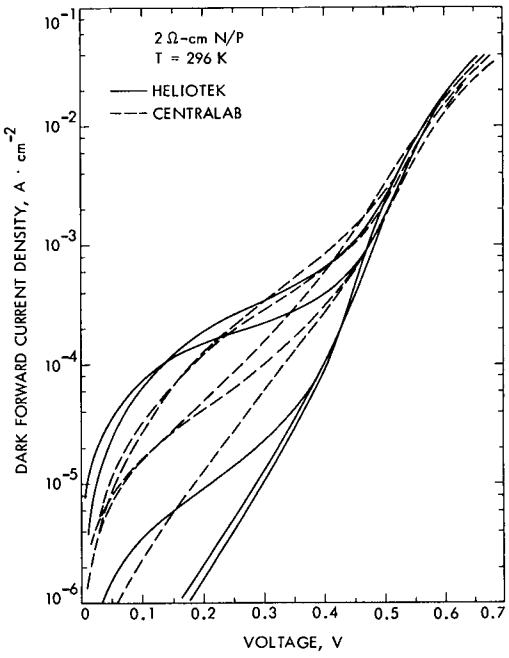

Fig. 7a. Dark forward current-voltage characteristics for typical 2- × 2-cm solar cells, 2-Ω-cm, T = 296 K

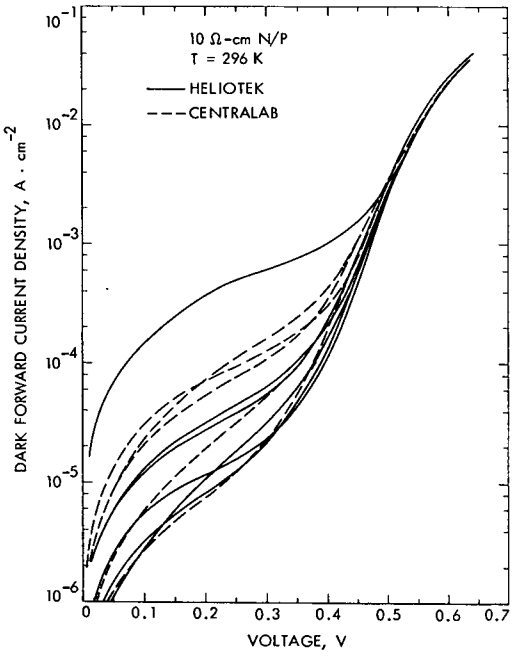

Fig. 7b. Dark forward current-voltage characteristics for typical 2- × 2-cm solar cells, 10-Ω-cm, T = 296 K

The usefulness, indeed the necessity, of measuring the junction characteristics on small individual areas of the solar cell is clearly evident in Fig. 8. This graph of I - V curves, using

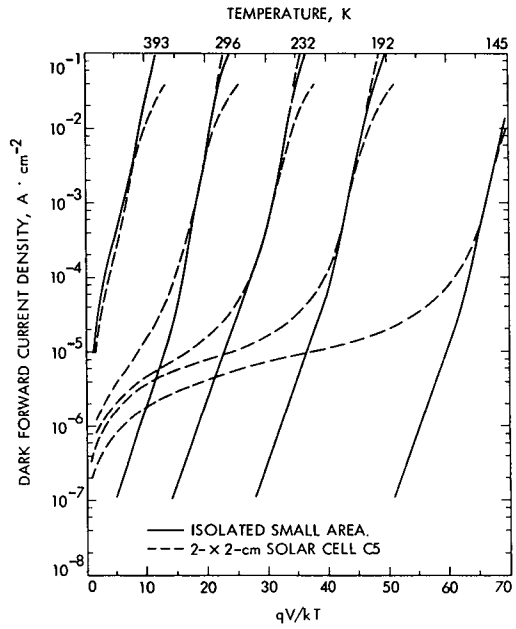

Fig. 8. Dark forward current-reduced voltage characteristics for a typical 10-Ω- cm, 2- × 2-cm solar cell and average small-area mesa

the reduced voltage qV/kT for five of the seven temperatures used in the present study, shows the large difference between measurements on a 2- × 2-cm cell compared to those on a small area of the same cell. Particularly at lower temperatures, since current shunting is essentially temperature independent, measurement of the smaller sloped portion of the I - V curve, which is indicative of the recombination current term, would be impossible on the larger area. An additional advantage of the small area measurements, which can be seen in Fig. 8, is that the current density that can be measured is about ten times higher than is possible in the 2- × 2-cm cell without significant voltage drop across the series resistance.

The relative uniformity of the forward characteristic of individual mesas as compared to those of 2- × 2-cm cells is shown in Figs. 9a and 9b for 2- and 10-Ω-cm material, respectively. The three 2- × 2-cm samples shown in Fig. 9a represent the range of shunt resistance found in

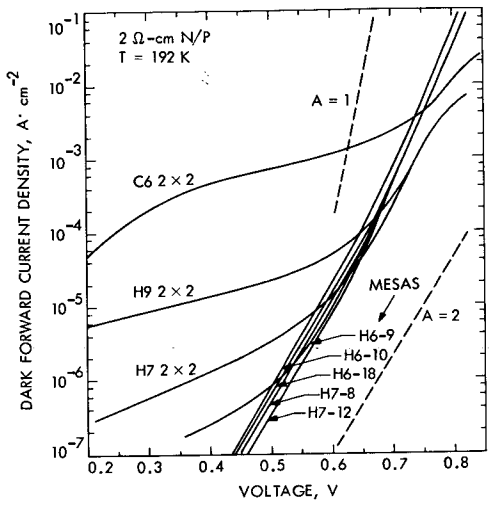

Fig. 9a. Dark forward current-voltage characteristics of some typical small-area mesas and 2- × 2-cm solar cells, 2-Ω-cm, T = 192 K

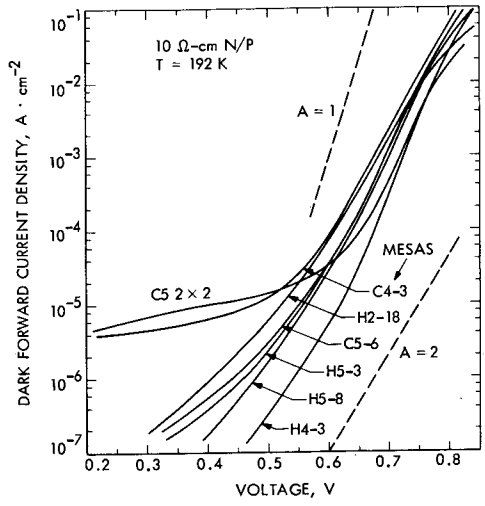

Fig. 9b. Dark forward current-voltage characteristics of some typical small-area mesas and 2- × 2-cm solar cells, 10-Ω-cm, T = 192 K

the 2-Ω-cm cells measured in this study (about 12 cells). In contrast, the individual mesa curves behave more consistently, especially in 2-Ω-cm cells. Other mesas measured, but not shown for reasons of clarity, had similar characteristics. Occasionally a mesa was found with shunting characteristics similar to a 2- × 2-cm cell (C4-3 in Fig. 9b), demonstrating that the shunting found in solar cells is localized in nature.

The results of computer least squares fitting the dark current data taken from mesas showing no shunting are summarized in Table 1. The data for the diffusion current component (I_{01}) were very similar for both Heliotek and Centralab cells, and thus, were averaged together. However, for the recombination current (I_{02}), the Centralab cells showed larger values and more variation between samples than did samples from Heliotek.

Table 1. Summary of reverse saturation current densities

T, K	Heliotek and Centralab I_{01}, A · cm^{-2}		Heliotek I_{02}, A · cm^{-2}		Centralab I_{02}, A · cm^{-2}	
	2 Ω-cm	10 Ω-cm	2 Ω-cm	10 Ω-cm	2 Ω-cm	10 Ω-cm
	9[a]	9[a]	5[a]	6[a]	4[a]	4[a]
393	1.21×10^{-7}	1.87×10^{-6}	2.57×10^{-6}	(1.0×10^{-4})[b]	1.4×10^{-5}	–
335	4.64×10^{-10}	2.57×10^{-9}	(3.9×10^{-7})	2.2×10^{-6}	(5.9×10^{-6})	1.0×10^{-6}
296	4.25×10^{-12}	1.65×10^{-11}	4.63×10^{-8}	8.27×10^{-8}	2.18×10^{-8}	4.78×10^{-8}
273	8.51×10^{-14}	3.05×10^{-13}	4.94×10^{-9}	3.72×10^{-8}	2.48×10^{-8}	6.5×10^{-9}
232	1.20×10^{-17}	5.00×10^{-17}	6.05×10^{-11}	3.60×10^{-9}	9.3×10^{-8}	4.0×10^{-9}
192	3.39×10^{-23}	2.17×10^{-22}	6.16×10^{-14}	1.28×10^{-12}	6.2×10^{-12}	5.5×10^{-11}
145	3.66×10^{-33}	8.88×10^{-32}	3.0×10^{-19}	3.4×10^{-18}	1.2×10^{-17}	3.1×10^{-17}

[a]Number of samples used for averaging.

[b]Parentheses denote values of greater uncertainty.

The least squares fitting procedure of Eq. (8) also provides values of A_1 and A_2. Values of A_1, which theoretically should equal one, were near that magnitude at room temperature, and in general, ranged from about 1 to 1.15. The magnitude tended to increase slightly with decreasing temperature, and were slightly higher for 10-Ω-cm material than for 2-Ω-cm. The values of A_2 generally varied from 1.8 to 1.9 in 2-Ω-cm material and from 1.9 to 2.7 in 10-Ω-cm material between 296 and 145 K. A_2 was difficult to extract at temperatures above room temperature, probably because of the very small relative amount of recombination current there, but indications are that values of $A_2 \lesssim 1.5$ give the best fit to the data. The more exact theory of Sah, Noyce, and Shockley (Ref. 6) does allow for values of $A_2 < 2$ when the dominant recombination center is not located at the exact center of the band gap and when the forward bias value is taken into account. Further analysis of the A-factor values is not being pursued until the least squares fitting program is modified to include current shunting.

Referring to Eqs. (2c) and (3), one sees that the temperature dependence of I_{01} can be given by the expression

$$I'_{01} = I'_{01} \exp (E_g/kT), \qquad (9a)$$

and that of I_{02} by the expression

$$I'_{02} = I'_{02} \exp (E_g/2kT), \qquad (10a)$$

since the exponential term dominates the temperature dependences of D_n, L_n, τ_0, N_c, and N_v. Therefore, an activation energy plot of I_{01} and I_{02} should give a slope of E_g and $E_g/2$, respectively. Figure 10 is such a plot for two small-area mesas, H 2-18 and H 6-10. The dashed and solid lines (2- and 10-Ω-cm material, respectively) are least squares-fitted linear lines using data from

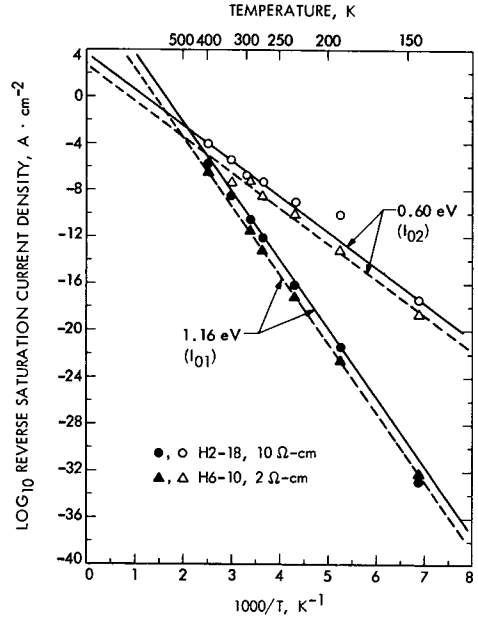

Fig. 10. Reverse saturation current densities I_{01} and I_{02} versus reciprocal temperature for 2- and 10-Ω-cm solar cells

all mesas measured. The data points given for the two samples are thus representative and will be used in the analysis below.

The linearity of the four lines in Fig. 10 shows that the representation given by Eqs. (9) and (10) is correct. The results of the least squares fit of the average data are for 2-Ω-cm solar cells

$$I_{01} = 2.3 \times 10^8 \exp (1.17/kT)\ A \cdot cm^{-2} \qquad (9b)$$

and for 10-Ω-cm solar cells

$$I_{01} = 6.4 \times 10^8 \exp (1.15/kT)\ A \cdot cm^{-2} \qquad (9c)$$

with room-temperature values of 2.6×10^{-12} and 1.5×10^{-11} A · cm^{-2}, respectively. The corresponding values for the recombination current components are for 2-Ω-cm solar cells,

$$I_{02} = 4.6 \times 10^2 \exp (1.21/2kT)\ A \cdot cm^{-2} \qquad (10b)$$

and for 10-Ω-cm solar cells,

$$I_{02} = 3.7 \times 10^3 \exp (1.19/2kT)\ A \cdot cm^{-2} \qquad (10c)$$

with respective room-temperature values of 2.4×10^{-8} and 2.7×10^{-7} A · cm^{-2}, respectively. The data from which I_{02} was calculated are that of solar cells manufactured by Heliotek. Data from Centralab solar cells, while comparable, had considerably more scatter.

The values of E_g obtained from the two components were 1.16 and 1.20 eV, the band gap of silicon. These values are only slightly higher than the accepted band-gap value of 1.12 eV at room temperature — rising to 1.16 eV at lower temperatures. The existence of the relations shown in Fig. 10 with the slopes given above is clear proof of a two-component nature of the diode current in silicon solar cells, i.e., current conduction by both diffusion of minority carriers (principally in the lightly-doped base region) and by recombination of minority carriers in the junction space-charge region.

Knowledge of the values of I_{01} and I_{02} along with other experimental data allows for calculations of diffusion lengths or lifetimes of minority carriers. Table 2 summarizes such calculations for the two samples used in Fig. 10. The built-in voltage V_{bi} and the doping in the base region N_A were obtained from the voltage dependence of the junction capacitance C, i.e., from the intercept and slope, respectively, of a plot of $(1/C)^2$ versus V (Refs. 2, 3). The width of the space-charge region W was obtained from the zero-bias value of the capacitance, assuming a simple parallel plate capacitance model. Use of Eq. (2c) and the value of I_{01} (296 K) given in Table 2 yielded a minority carrier lifetime of 4.4 and 7.1 μs for 2- and 10-Ω-cm base material, respectively. The corresponding diffusion lengths are 123 and 163 μm. The lifetime values fall well within the range of the lifetimes found by independent measurements in finished silicon solar cells.[3] The longer diffusion length in 10-Ω-cm material is also expected because of its greater purity.

[3] Iles, P., private communication.

Table 2. Physical parameters and calculated junction parameters of two representative mesas

	Units	H6-10	H2-18
Resistivity ρ	Ω-cm	2	10
Doping N_A (from C-V)	cm^{-3}	7.2×10^{15}	1.8×10^{15}
Built-in voltage (from C-V)	V	0.850	0.705
Junction capacitance	$fd \cdot m^{-1}$	2.7×10^{-4}	1.5×10^{-4}
Junction width W	μm	0.39	0.70
Diffusion constant D_n	$cm^2 \cdot s^{-1}$	35	38
I'_{01} (1/T = 0), Eq. (9)	$A \cdot cm^{-2}$	1.4×10^{9}	1.3×10^{9}
E_g (fit), Eq. (9)	eV	1.19	1.16
I'_{02} (1/T = 0), Eq. (10)	$A \cdot cm^{-2}$	7.4×10^{1}	3.8×10^{3}
E_g (fit), Eq. (10)	eV	1.15	1.19
I_{01} (296 K)	$A \cdot cm^{-2}$	6.3×10^{-12}	2.0×10^{-11}
I_{02} (296 K)	$A \cdot cm^{-2}$	1.2×10^{-8}	2.8×10^{-7}
Diffusion length L_n	μm	123	163
$\tau_n = L_n^2/D_n$	s	4.4×10^{-6}	7.1×10^{-6}
τ_0, Eq. (7)	s	2.7×10^{-6}	0.2×10^{-6}

Similar calculations using Eq. (7) yielded values of the effective lifetime τ_0 as given in Table 2. These values bear no relationship to the values of the diffusion lifetimes τ_n. Surprisingly, the value of τ_0 for 10-Ω-cm material is more than ten times shorter than the value for 2-Ω-cm material. The latter fact may indicate that multi-level recombination centers are involved in determining the magnitude of I_{02} and that the simple expression $\tau_0 = \sqrt{\tau_n \tau_p}$ is not valid here. Another possible explanation involves the impurity gettering ability of the P2O5 diffusion process. It has been observed (Ref. 8) that natural gettering of deep impurities like gold, iron, or copper by the glassy substance formed on the surface during the diffusion of phosphorous causes a build-up in the deep impurity concentration near the surface (<few microns) one to two orders of magnitude larger than the original concentration in the bulk! The lower lifetime τ_0 in 10-Ω-cm material might be explained by this mechanism if the gettering "efficiency" is higher in more pure (shallow level impurities like boron) material than it is in less pure material. Further investigations of τ_n and τ_0 over a wider range of base resistivities are planned.

B. Current Shunting and Nonuniform Recombination Current

The effect of shunting paths and recombination currents on the dark forward I-V characteristic were earlier shown in Figs. 2-5. Their effect on the illuminated solar cell output characteristic will be demonstrated in Part II of this report where it will be shown that even typical amounts of shunting and recombination current can lower the cell efficiency by up to 30% at low light intensities. That the shunting is localized was clearly demonstrated by the fact that only rarely were small area mesas found with any shunting.

The most likely cause of these shunts would be scratches penetrating through the junction region, since in solar cells, the junction is only 0.3 to 0.5 μm from the surface. If this is so, any metallization on this surface with subsequent firing should increase the amount of shunting. Such a metallization process is performed, of course, when the grids are placed on the solar cell. This process, designed principally for obtaining low resistance contacts on the lightly doped back surface, involves the evaporation of about 0.1 μm of titanium before a thicker film of silver is evaporated. The contact is then fired at about 600°C in a hydrogen atmosphere so as to react the titanium with the natural oxide layer on the silicon.

To investigate the possible effect of such a process on current shunting, seven Centralab 2-Ω-cm solar cells, which had been processed normally including the usual grids, had their entire front surface coated with the Ti/Ag metal films. All seven had typical current-voltage characteristics when measured. When, however, four of the samples were sintered in the manner done for forming the back contact and grid, the amount of shunting increased dramatically as

shown in Fig. 11a. Samples CS 1 – 4 were sintered and samples CU 1 – 3 were left unsintered as controls. The dashed line represents an idealized 2- × 2-cm cell with no shunting using the average values of I_{01} and I_{02} found in the small area mesas. Hence, it appears that much of the shunting in ordinary cells may occur because of the use of fired titanium under the grid lines and bar contact. The randomness of the shunting paths would

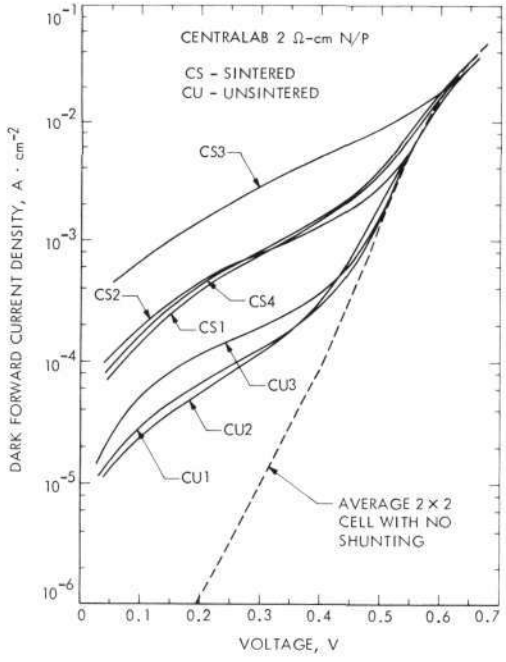

Fig. 11a. Dark forward current-voltage characteristics of Centralab solar cells with full front Ti/Ag contacts

then seem to come from both the randomness of scratches inflicted after diffusion, and from the random chance of a grid line overlapping such a scratch. Figure 11b shows the results of a similar experiment with Heliotek cells, except that here the unsintered cells did not have the preliminary sintering of the back contact and grid lines. Thus, two of the cells, HU 2 and HU 3, show very high series resistance and the effect of a Schottky barrier at the back contact. However, it is clearly seen that initially, for this particular grouping, the amount of shunting was significantly lower than that found in the Centralab cells, and that the effect of sintering was much less than that found in the Centralab cells. The implication is that on the average the Heliotek cells are less prone to current shunting. This is also evident in Figs. 7a and 7b, though some Heliotek cells show rather significant shunting.

Further evidence of current shunting due to scratches in the diffused region was obtained from scanning electron microscope pictures of a mesa that had shown shunting characteristics. Figure 12a is a picture of the mesa using the electron beam induced conductivity (EBIC) mode. In this mode, electron-hole pairs are formed by the primary electron beam (10 kV) just as they are by photons. The penetration depth of 10 kV electrons in silicon is about 1 μm. Hence, most of the current measured (scanned and displayed much as by

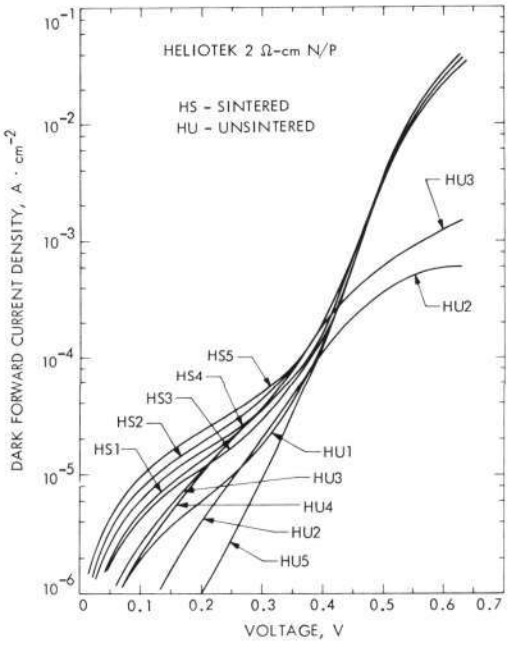

Fig. 11b. Dark forward current-voltage characteristics of Heliotek solar cells with full front Ti/Ag contacts

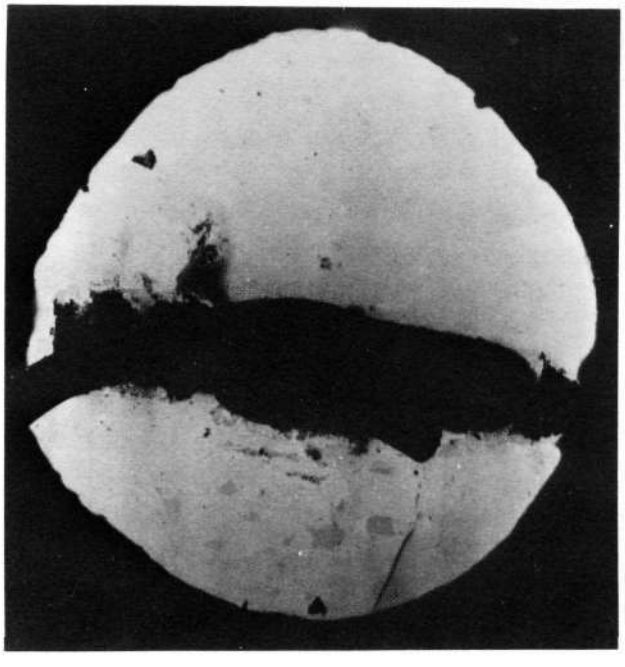

Fig. 12a. Scanning electron microscope picture (electron beam induced conductivity mode) of mesa with scratch (X60)

a vidicon tube) is due to the collection of minority holes from the diffused region. The dark central line is the original grid line with a wire soldered to it. At the bottom of the picture is seen a dark linear feature. (The other dark areas are due to surface debris.) The feature breaks into a discontinuous line approaching the grid, but may

continue under the grid. A higher magnification picture using the collected secondary electrons that are emitted from the surface is shown in Fig. 12b. This mode gives a picture much like that seen with an optical microscope but with far more depth-of-field. The picture shows that the linear feature is indeed a scratch that has penetrated the junction region, perhaps accounting for the abnormal amount of current shunting. A lower magnification EBIC picture of a different cell also shows numerous linear features, some of them running under grid lines (Fig. 13).

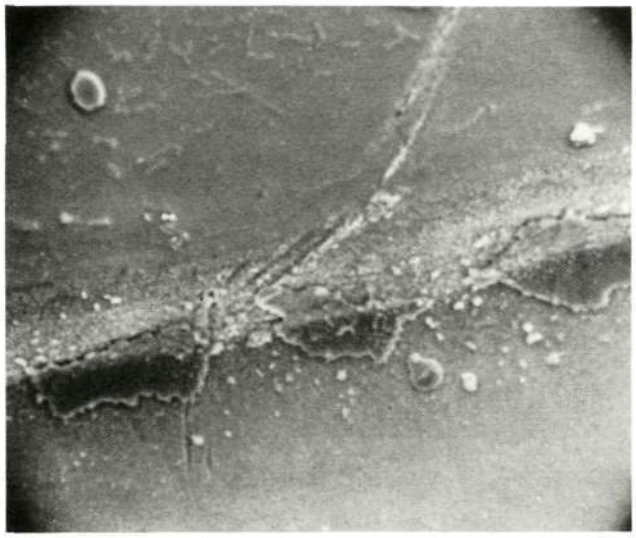

Fig. 12b. Scanning electron microscope picture (secondary electron emission) of mesa edge with scratch (X1200)

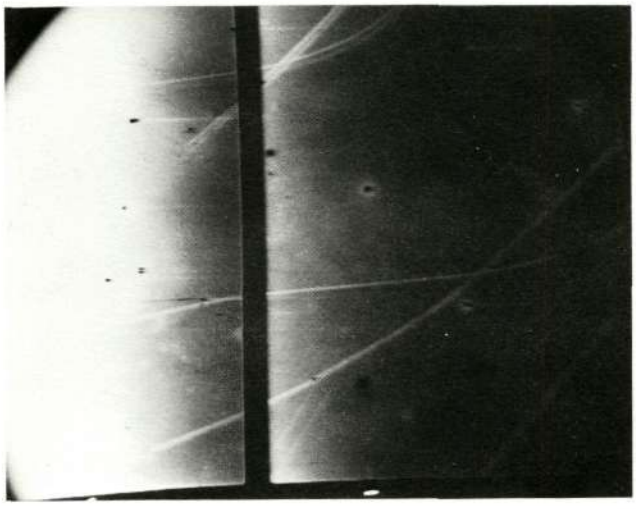

Fig. 13. Scanning electron microscope picture (electron beam induced conductivity) of part of a solar cell showing linear features

Previously, reference was made to some small-area mesas that seemed to show values of recombination current higher than the average. To further check the possibility of nonuniformity in I_{02} across the plane of the cell junction, a montage of a solar cell was made with the scanning electron microscope before individual mesas were etched from it. Figure 14a is a montage using secondary electron emission that shows a surface

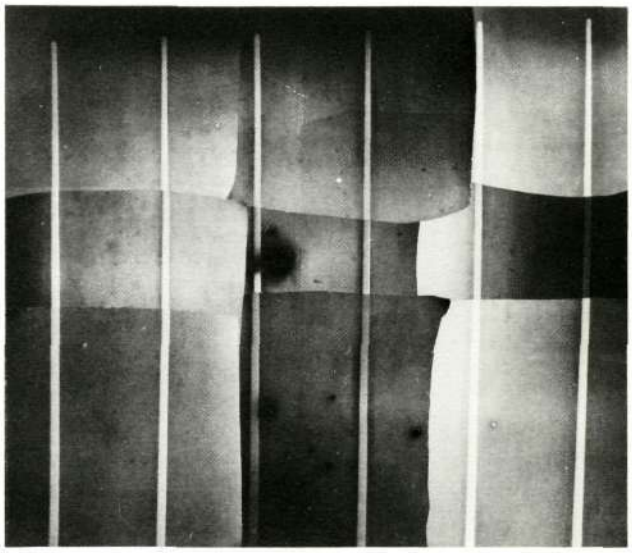

Fig. 14a. Scanning electron microscope montage of a solar cell (secondary electron emission)

free of all but a few particles. However, when a montage of the same cell is made in the EBIC mode as shown in Fig. 14b, structure appears that indicates a high degree of variability in current collection by the junction. (The light areas are regions of lower current collection.) Since all of the primary electrons are absorped in the first micron of silicon, most of the structure seen must be due to defects in the diffused region. The crater-like and ridge depressions that appear

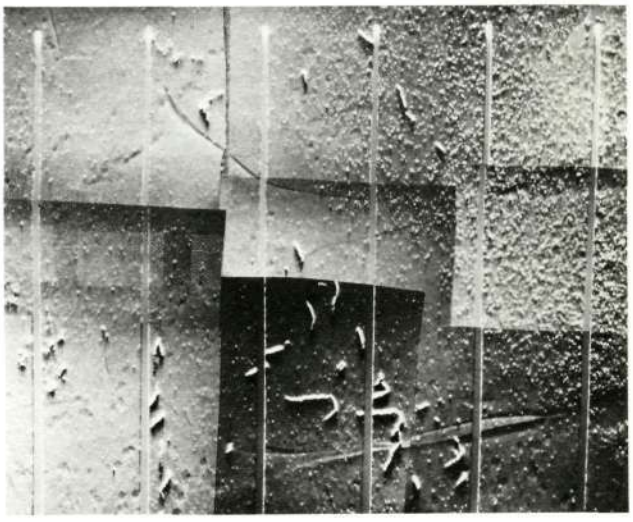

Fig. 14b. Scanning electron microscope montage of same solar cell as in Fig. 14a (electron beam induced conductivity mode)

are not easily explained at this time, but the "salt pattern", which is denser on the right side, could possibly be explained by precipitates. High densities of precipitates in high-purity, low-oxygen content silicon that have been identified as copper have been recently reported (Ref. 9). In crucible-grown silicon, which normally has an oxygen content of $\gtrsim 10^{16}$ - 10^{17} cm^{-3}, and from which most solar cells are made, precipitates of SiO_2 have also been reported that can affect the "softness" of the reverse characteristic (Ref. 10).

A number of mesas were etched from the cell used for Figs. 14a and 14b in such areas where the most prominent structure appears, as well as in some areas relatively free of such structure. Only minor differences were detected between the mesas in the dark forward I - V curves, except that a mesa in the upper righthand area of the cell showing the highest concentration of precipitate-like patterns did have significantly higher recombination current.

V. CONCLUSIONS AND RECOMMENDATIONS

Precise values of the reverse saturation currents in silicon solar cells and magnitudes of the diffusion and recombination components have been obtained. The magnitude of the diffusion current was shown to be that predicted by Shockley's theory. The recombination current, as well as leakage current due to shunting, were shown to be nonuniform across the solar cell. Models were given demonstrating the effect of recombination and shunting currents on the dark forward current-voltage characteristic.

At least one cause of current shunting in solar cells is apparently due to surface scratches penetrating through the junction region. The elimination of these and of regions showing higher magnitudes of recombination current can raise conversion efficiencies by up to 50% in solar cells in Jupiter-type environments. Cells used for deep-space missions beyond the orbit of Mars should be processed to minimize these effects. Elimination of the titanium interlayer on the front surface of the solar cell (junction side) should considerably reduce the amount of shunting. The high surface carrier concentration on the diffused side should allow for good ohmic contacts using only the silver metallization. The use of aluminum alloyed p^+ back contacts will eliminate the need for any titanium evaporation as well as eliminate possible Schottky barrier contacts at lower temperatures. Shunting could be further minimized by reducing the area of the front contacts since the much lower current densities encountered in solar cells operating between 2 and 5 AU relaxes the series resistance problems considerably. An obvious additional advantage of such a reduction is the increased current output, and hence, increased efficiency, due to the larger area for light absorption.

Testing and qualifying solar cells in solar simulators at low temperatures is time consuming and expensive. These costs could be substantially reduced by preliminary screening of solar cells to be used in low-intensity, low-temperature missions by measuring their dark forward current-voltage characteristics at room temperature and specifying upper limits on the current at lower voltages.

To further explore the possible causes of nonuniform current collection by the junction and the nonuniformity and excessive magnitudes of recombination current, further testing of solar cells made under controlled, but variable, conditions of diffusion processes such as temperature uniformity, and quenching rates should be made. The use of the scanning electron microscope and X-ray topographic instrumentation would be of great aid in such investigations.

REFERENCES

1. Wolf, M., and Rauchenback, H., "Series Resistance Effects on Solar Cell Measurements," Advan. Energy Convers., Vol. 3, p. 455, 1963.

2. Grove, A. S., Physics and Technology of Semiconductor Devices, Chapter 6. John Wiley and Sons, Inc., New York, 1967.

3. Sze, S. M., Physics of Semiconductor Devices, Chapter 3. John Wiley and Sons, Inc., New York, 1969.

4. Reference (3), Chapter 12.

5. Rappaport, P., and Wysocki, J. J., Photoelectronic Materials and Devices, Chapter 6. Edited by S. Larach. D. Van Nostrand Comp., Inc., Princeton, N. J., 1965.

6. Sah, C., Noyce, R. N., and Shockley, W., "Carrier Generation and Recombination in P - N Junctions and P - N Junction Characteristics," Proc. IRE Vol. 45, p. 1228, 1957.

7. Sah, C., "Effect of Surface Recombination and Channel on P - N Junction and Transistor Characteristics," IRE Trans. Electron Devices, Vol. ED 9, p. 94, 1962.

8. Nakamura, M., Kato, T., and Oi, N., "A Study of Gettering Effect of Metallic Impurities in Silicon," Jap. J. Appl. Phys., Vol. 7, p. 512, 1968.

9. Ness, E., and Lunde, G., "Copper Precipitate Colonies in Silicon," J. Appl. Phys., Vol. 43, p. 1835, 1972.

10. Batavin, V. V., "Influence of SiO_2 Precipitates on the Current-Voltage Characteristics of p - n Junctions in Solid Silicon," Sov. Phys. – Semicond. Vol. 4, p. 641, 1970.

NASA – JPL – Coml., L.A., Calif.